F. Ferrari, M. Lavagna
Ballistic Landing Design on Binary Asteroids: the Aim Case Study
Advances in Space Research, Vol. 62, N. 8, 2018, p. 2245-2260
doi:10.1016/j.asr.2017.11.033

Ballistic landing design on binary asteroids: the AIM case study

Fabio Ferrari*, Michèle Lavagna

Department of Aerospace Science and Technology, Politecnico di Milano, Via La Masa 34, 20156, Milan, Italy

Abstract

The close-proximity exploration of small celestial bodies of our Solar System is the current frontier of space exploration. Trajectory design and exploitation of the natural dynamics around such bodies represents a very challenging astrodynamics problem, due to their weak and highly chaotic gravitational environment. The paper discusses design solutions for the ballistic landing of a small and passive probe, released to land on the smaller of a binary asteroid couple. The work is focused on the Asteroid Impact Mission (AIM) case study, although the methods and analyses presented are general and applicable to any binary asteroid scenario. The binary system is modeled using a shape-based three-body problem and three-body solutions are investigated within the Didymos binary system. Manifold dynamics near libration points associated to the asteroid three-body system are exploited to find low-energy and high-success landing trajectories. The validity of implemented approach and solutions found are discussed and results in terms of success rate and landing dispersion are shown.

Keywords: landing; binary asteroid; shape model; Didymos; AIM; MASCOT-2

1. Introduction

Due to the large accessibility of the Near Earth Asteroid (NEA) population to spacecraft, rendezvous missions to small celestial bodies of our Solar

*Corresponding author

Email address: fabio1.ferrari@polimi.it (Fabio Ferrari)

System are the current frontier of space exploration. Motivated by a great scientific interest and invaluable technological demonstration opportunities, the close-proximity exploration of asteroids and comets is among the latest challenges of modern astrodynamics. Due to their peculiar and irregular mass distribution, the gravity field around such celestial bodies is characterized by an extremely nonlinear and chaotic dynamical behavior.

Among the small body population, binary asteroid systems are of great interest since 1993, when the first natural satellite of an asteroid was discovered. At that time the Galileo spacecraft imaged the asteroid moon Dactyl while performing a flyby near its bigger companion 243 Ida (Belton et al., 1994). In the last few decades, many multiple asteroid systems were discovered and it is currently estimated that about 16% of NEA are binaries (Margot et al., 2002; Merline et al., 2002). The study of binary asteroids can be very interesting under many points of view. These kinds of systems possess peculiar properties that make them good candidates for scientific and technological studies. The binary asteroid environment is the ideal place to study gravitational dynamics, to enhance the understanding of how celestial bodies in the Solar System were formed and how they evolve. More in detail, they offer the unique opportunity to determine precisely asteroid masses and densities: nowadays, mass and density are accurately known only for a few tens of small body objects. In case of binary systems, the mass of the asteroids can be accurately computed after the orbit of the satellite object is measured (Bottke Jr. et al., 2002). Binary systems represent an ideal place for technology demonstration missions, as a test bench for In-Orbit-Demonstrations (IOD) experiments. For these many reasons, the study of the dynamical environment near an asteroid pair is an extremely relevant topic for future missions design.

The paper discusses the design options for a ballistic landing on the secondary of Didymos binary system, with explicit reference to the Asteroid Impact Mission (AIM) (Ferrari et al., 2016a; Cheng et al., 2015) case study. The mission analysis strategy is outlined and taylored to the peculiar dynamics and requirements related to the AIM mission. Relevant design parameters are identified and their effect on the ballistic landing design is discussed. Expected landing results and proposed mission analysis design solution are also presented. The target is the near-Earth binary asteroid 65803 Didymos (Scheirich and Pravec, 2009). In the following, the primary asteroid is informally called Didymain, while its small companion is called Didymoon.

The mission scenario considers a small lander, named MASCOT-2, to be

released on Didymoon's surface, to perform the Moonlet Engineering eXperiment (MEX) that will demonstrate the ballistic landing and operations of a miniaturized asteroid lander on a binary system. MASCOT-2, a very small (about 13 kg) and completely passive probe, is named after MASCOT (Mobile Asteroid Surface sCOuT), the lander on board the Hayabusa-2 mission (Tsuchiyama et al., 2011; Ulamec et al., 2014). The problem of landing a space probe on such celestial bodies is nowadays being studied for the first time and the related research field is very young. The Rosetta mission (Taylor et al., 2015) highlighted the challenges of designing close proximity trajectories and landing a probe on the surface of an extremely irregular body such as comet 67P/Churyumov-Gerasimenko (Sierks et al., 2015), whose shape and mass distribution were completely unknown and unexpected during the mission design phase. In that case, the Philae lander (Biele and Ulamec, 2008) release was challenged by the highly perturbed dynamical environment in the proximity of the comet and by its very low and irregular gravity field. In analogy to the Rosetta mission, the AIM case study entails the release of a small and passive probe that will reach the surface of a largely unknown object after a purely ballistic descent. MASCOT-2 lander does not feature any mechanism to anchor to the surface of the asteroid, which makes the landing design even more challenging. Moreover, Didymos system's gravity field is expected to be weaker, with an escape velocity from Didymoon's surface of few cm/s, since the asteroids are estimated to be nearly two (Didymain) and four (Didymoon) orders of magnitude less massive than comet 67P/Churyumov-Gerasimenko. In addition, the presence of two gravitational attractors makes the dynamics in the close proximity of the couple highly unstable and chaotic. The accurate knowledge of the dynamics driving the motion of a body in the vicinity of such a binary system is then a key point for the success of the mission, to correctly operate scientific payloads and to effectively land the probe on the asteroid.

An effective strategy for MASCOT-2 release is proposed here. The increased complexity of having two small bodies as gravity source is used here as a potential opportunity to be exploited in the design process, through the use of three-body modeling techniques. The AIM/MASCOT-2 scenario is presented in the following paragraphs as a case study. However, the applied methodology is representative for any asteroid/small body scenario.

2. Dynamics

The dynamics of MASCOT-2 in the proximity of the binary asteroid system are modeled using the Restricted Three-Body Problem (R3BP), with shape-based models to reproduce the gravity field generated by the two asteroids.

2.1. Asteroid models

Few strategies are usually adopted to model the gravity field about asteroids. Classic methods consider harmonic expansion of gravitational potential (Kaula, 1966) to model the irregularities of a simple Keplerian field. Shape-based methods are used to model the asteroid as objects with specific shapes, such as homogeneous ellipsoids (Scheeres, 1994) or polyhedra (Werner and Scheeres, 1997; Scheeres et al., 1998): in this case their distribution of mass is not spherical and the gravity field in its proximity is computed accordingly. Other methods use a number of masses (mascon models) to reproduce the mass distribution of the body. The mascon method was first developed to explain the anomalies of the Moon's gravity field by Muller and Sjogren (1968). The inclusion of concentrations of mass in the nearly spherical mass distribution of the Moon helped in the development of a highly accurate lunar gravity model. A similar technique is used to reproduce the gravity field of asteroids (Colagrossi et al., 2016; Ferrari et al., 2017; Geissler et al., 1996). The applicability of each method depends on the information available on the body's mass distribution and on the level of accuracy required by the application. Typically, each model fits a specific class of asteroids and application range. In general, the determination of mass and bulk density of small body is a very difficult task (Hilton, 2002) and very little is known about their internal mass distribution.

According to the latest observations of Didymos system, information on the shape of the asteroids are partially available. A face-vertex shape model of Didymain is available[1], while Didymoon's shape is estimated to be an elongated tri-axial ellipsoid. The implementation is based on the methods proposed by Werner and Scheeres (1997) and Scheeres (1994). The gravity effects of the asteroids are modeled using their shape model and their

[1]The Didymain shape model is used in the frame of ESA's AIM contract, however it is still unpublished (courtesy of L. Benner and S. Naidu)

mass distributions are considered to be uniform (constant density polyhedron/ellipsoid).

2.2. Didymos modified CR3BP

Few strategies have been adopted in the past to model the dynamics around binary systems, using non-Keplerian techniques to model the gravity effect due to asteroids. Scheeres and Bellerose (2005); Bellerose and Scheeres (2008a,b) used the Full Restricted Three-Body Problem to model the mutual interaction between the asteroids, while Gabern et al. (2006); Ferrari et al. (2016b) used lumped models to reproduce the mass distribution of the primary. In all cases, because of the presence of two gravitational sources, the dynamics in the neighborhood of the binary system is naturally modeled as an R3BP. The dynamical model implemented in this work starts from the same consideration and it is classified as a restricted three-body problem. More in detail, the dynamical system is based on the Circular Restricted Three-Body Problem (CR3BP) formulation, refined by including the effects of non-spherical mass distribution when modeling the two asteroids. Didymain and Didymoon are the primaries of a three-body system and their motion is constrained on circular paths around the barycenter of the binary. The classical CR3BP models the primaries using spherical and uniform mass distribution around their center of mass, which is equivalent to consider point-mass sources. For this reason, the classical CR3BP accurately describes the dynamics around the binary couple only if the mass distribution of the two asteroids is close to be spherical. In general, this is not the case for small celestial bodies. The highly irregular mass distribution of such bodies can lead to very inaccurate results when studying the dynamics in their close proximity. In this work, more accurate models are implemented within a modified CR3BP, by including information on more complex mass distribution into the classical CR3BP. As for the case study, due to the lack of information and direct measurements regarding the mass distribution of the asteroids, the latter is directly recovered from shape information: the mass is considered to be uniformly distributed, within a non-spherical shape of the asteroid. Since it deals with the well-known CR3BP formulation, this strategy takes advantage from the large availability of dynamical solutions for astrodynamics and mission analysis design, by adapting such solutions to the case of modified CR3BP.

The working assumptions of the CR3BP related to the dynamics of the primaries are kept. The two asteroids follow a two-body circular path around

the barycenter of the binary and their motion is not influenced by the presence of the third body (MASCOT-2). As usual, the equations of motion of the third body are written in the synodic frame, which rotates together with the primaries (Szebehely, 1967). Concerning the rotational motion of Didymoon, observations show that the secondary is in a tidally-locked configuration, having the same period of rotation about its axis and revolution about the barycenter of the binary system. This configuration is such that Didymoon shows the same face to Didymain during its motion and Didymoon's smaller principal axis of inertia is aligned to the Didymoon-Didymain direction. The relative configuration between the two primaries is fixed as seen from the three-body synodic frame. With reference to Figure 1, Didymoon's smaller principal axis lies on the x axis of the rotating frame, together with the centers of mass of the primaries, which have fixed position in this frame. Their nondimensional $\tilde{x}$ coordinates are $-\mu$ and $1-\mu$, where parameter μ is the mass ratio between the primaries, whose masses are referenced as M_1 and M_2

$$\mu = \frac{M_2}{M_1 + M_2} \tag{1}$$

Figure 1 shows Didymos three-body system as seen from the rotating frame, in dimensional coordinates.

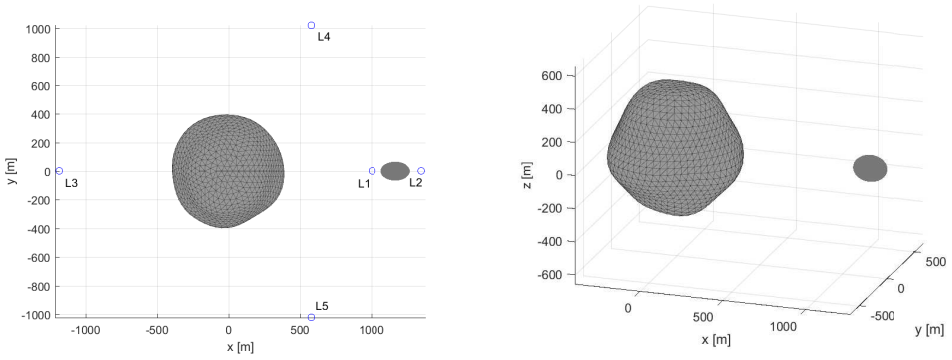

(a) (b)

Figure 1: Didymos three-body system in rotating dimensional frame (a) x-y plane view with libration points (b) three-dimensional view.

The nondimensional equations of motion of the spacecraft are written in

the synodic frame as

$$\begin{cases} \ddot{\tilde{x}} = \tilde{x} + 2\dot{\tilde{y}} + \tilde{U}_{\text{poly}_{\tilde{x}}} + \tilde{U}_{\text{ell}_{\tilde{x}}} \\ \ddot{\tilde{y}} = \tilde{y} - 2\dot{\tilde{x}} + \tilde{U}_{\text{poly}_{\tilde{y}}} + \tilde{U}_{\text{ell}_{\tilde{y}}} \\ \ddot{\tilde{z}} = \tilde{U}_{\text{poly}_{\tilde{z}}} + \tilde{U}_{\text{ell}_{\tilde{z}}} \end{cases} \tag{2}$$

where the subscript $(\cdot)_{\tilde{x}}$, $(\cdot)_{\tilde{y}}$ or $(\cdot)_{\tilde{z}}$ indicate partial derivatives, superscript $\tilde{}$ indicates nondimensional coordinates, $\tilde{U}_{\text{poly}}$ and $\tilde{U}_{\text{ell}}$ represent the nondimensional gravitational potential due to the primaries Didymain (also referenced as P_1) and Didymoon (P_2). As for the classical CR3BP formulation $\tilde{U}_{\text{poly}}$ and $\tilde{U}_{\text{ell}}$ include both the gravitational potential due to primaries and the effect of synodic frame rotation. The classical CR3BP formulation considers point-mass (or spherical) gravitational potentials, while the modified version of the CR3BP implements shape based models of the two asteroids, nondimensionalized according to characteristic length L^* and time t^* associated to the problem. Note that only gravity terms due to the primaries acting on the third body are modified compared to the classical CR3BP formulation. No changes are made on the assumptions regarding the motion of the center of mass of the two primaries and their mutual interaction.

2.3. Model validity

Since the gravity field is extremely low, it is in general worth to consider the effects of orbital perturbations due to Solar Radiation Pressure (SRP) and fourth-body effect (Sun or Earth). Table 1 reports the order of magnitude of orbital perturbations acting on the lander, as compared to Didymos gravity acceleration at 1 km from the primary. The most relevant perturbing effect is the SRP and it is three orders of magnitude less important than Didymos gravity. Accordingly, the SRP could be relevant only in case of long time of flights. This is not the case for MASCOT-2, which is foreseen to only have a short ballistic descent of a few hours before reaching the surface of Didymoon. Fourth body perturbations due to Sun and Earth (which is closer than 0.1 AU during MASCOT-2 descent) are shown not to be relevant at all.

The most important source of perturbation will likely be the irregularities of Didymain and Didymoon gravity fields, which act in a very relevant way on MASCOT-2 dynamics during its ballistic descent. Figure 2 shows an example of landing trajectory, propagated using different models of the Didymain-Didymoon gravity field. Dotted-dashed line indicate the trajectory in the classical CR3BP model. In this case, the mass distribution of both Didymain

Table 1: Dynamical effects acting on MASCOT-2 in the proximity of Didymos system

	Order of magnitude [m/s^2]
Didymos gravity	10^{-5}
SRP	10^{-8}
Sun's gravity (4^{th} body)	10^{-11}
Earth's gravity (4^{th} body)	10^{-13}

and Didymoon is modeled as a uniform sphere (central field). This case is referenced in the figure as S1-S2. The second case is referenced as S1-E2 and refer to modeling Didymain as a sphere and Didymoon as an ellipsoid. The last case is the most accurate and it is the one implemented in this work and discussed above: P1-E2, with polyhedral model of Didymain and ellipsoidal model of Didymoon.

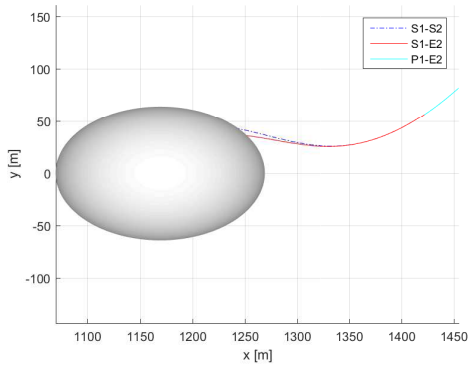

Figure 2: Ballistic descent with different models of Didymain-Didymoon gravity: sphere-sphere (S1-S2), sphere-ellipsoid (S1-E2), polyhedron-ellipsoid (P1-E2).

Figure 2 shows that a significant difference exists in the final trajectory when comparing different modeling strategies of Didymoon, while much lower discrepancy is observed when modeling Didymain as a sphere or using the polyhedron model.

3. Ballistic landing design

MASCOT-2, as its predecessor MASCOT (on board the Hayabusa mission), is a completely passive probe. It does not have any device to stop or anchor on Didymoon's surface once there. Also, MASCOT-2 does not have

any orbit-controlling device, such as thrusters. For this reason, the landing trajectory must be carefully designed, and a well-designed purely ballistic descent is the only chance to reach Didymoon's surface. The success of the landing is completely depending on the choice of the release condition. Moreover, the safety of AIM spacecraft must be ensured during all phases of the mission, meaning that the release point shall be far enough from both asteroids. Given these requirements, two major criticalities are identified for the MASCOT-2 scenario. The first critical aspect regards the capability of the lander to reach the surface of Didymoon after release. This is an extremely challenging problem under the dynamical environment described above. A small deviation in the release state could lead to very different trajectories, which might or might not intersect Didymoon's surface. To avoid this problem, the landing trajectory shall be confined in a region with low divergence of the dynamical flow. The second challenge related to the MASCOT-2 landing design appears clearly linked to whether the lander will stay or not on the surface after touch down. The extremely low-gravity environment will likely induce the probe to bounce multiple times until reaching a stable position on Didymoon's surface or, in the worst condition, to escape from the asteroid's gravity field. For this reason, the lander shall be put on a suitable trajectory, that allows the lander to safely reach Didymoon with a sufficiently small touch down velocity, such that it will not bounce away. From the design point of view, the touch down velocity plays a major role, especially when compared to the local escape velocity at the asteroid surface.

3.1. Three-body escape velocities

In order to better understand the dynamical behavior of the third body in such peculiar environment, it is worth to highlight the role of the escape velocity and identify the main design options for the case study. In the frame of the classical restricted two-body problem, the escape velocity is defined as the minimum velocity to escape from the gravitational attraction of the body. In this case, the limiting condition corresponds to the velocity to be inserted on a parabolic arc, which reaches the Sphere Of Influence (SOI) of the attractor after infinite time. Conversely, this means that a body release at the SOI, heading towards the attractor through a pure ballistic descent, will reach its surface with a touch down velocity greater or equal than the minimum escape velocity. This imposes a dynamical constraint to the minimum touch down velocity reachable from outside the SOI. The only way to decrease the touch down velocity with a pure ballistic descent is to

release the probe from within the SOI, in order to let the probe withstand to the gravitational acceleration for a smaller time span. As for the case of Didymos system and when Didymoon's rotation is taken into account, the minimum escape velocity from Didymoon's surface occurs at the equator and it is slightly lower than 8 cm/s. The SOI with respect to the main attractor (Didymain), is approximately 180 m, which corresponds to nearly 100 m altitude from Didymoon's surface. As mentioned, this is valid for the case of restricted two-body problem formulation, which can lead to very inaccurate results in the Didymos case of study.

Analogous concepts can be derived for the case of restricted three-body problem. The R3BP is known not to have an analytical solution of the equations of motion and, unlike the case where a single attractor is present, the escape velocity from Didymoon's surface differs depending on the local latitude and longitude. When dealing with R3BP, it is common to look at the qualitative behavior of the motion of the third body using the energy approach. More in detail, zero relative velocity surfaces (Hill's curves) can be derived to qualitatively bound the motion of the particle in the proximity of the two primaries (see Szebehely (1967); Schaub and Junkins (2003) for further detail). Interesting insights on MASCOT-2 scenario can be derived by following this approach. Analogously to the two-body case, it is possible to define the escape velocity as the minimum velocity allowing a massless body to escape from Didymoon's surface. For a sufficiently low amount of energy, zero relative velocity surfaces will separate clearly the region near P_1 from the region near P_2: in this case, a body near P_2 is trapped to stay in its neighborhood. For a higher energy level, a connection between the two zero relative velocity surfaces opens in correspondence of the L1 point: in this case, the particle is allowed to move between P_1 and P_2 regions, by passing through the L1 neck. With relation to MASCOT-2 scenario, this condition can be seen as the lowest energy for a particle to escape from Didymoon's neighborhood. Figure 3 shows an example of low energy trajectory escaped from Didymoon through the L1 neck.

More in detail, the lowest energy trajectory to escape from P_2 region is the stable manifold associated to L1 point. The velocity at intersection between the manifold and the surface of Didymoon corresponds to the minimum escape velocity from Didymoon's surface. This kind of information can be used to assess the existence of a ballistic landing trajectory, from outside the P_2 region. With analogy to the escape problem, a lander can reach the surface from L1 through its unstable manifold. Both landing and escaping trajecto-

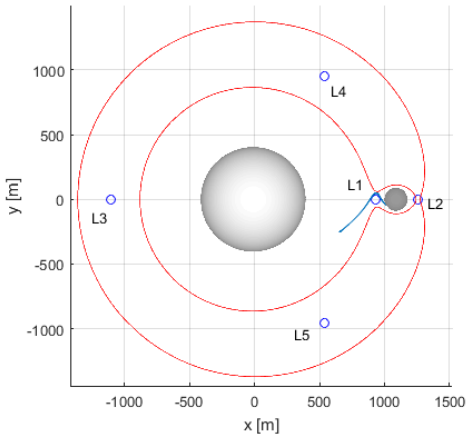

Figure 3: Low energy escape from Didymoon through the L1 neck of Hill's curves.

ries are found at the same level of energy, corresponding to the opening of the L1 neck. Intuitively, the minimum energy correspond to the minimum escape velocity from Didymoon's surface. In the following, this velocity will be referenced as L1 escape velocity, or v_{L1}. As for the case of Didymos, this trajectory corresponds to an escape velocity v_{L1} of about 4.57 cm/s. In analogy to what was discussed for the two-body case, this value represents the minimum touch down velocity when the probe is released from L1 point. It is known that a higher level of energy allows the opening of the L2 neck. In this case, the particle has enough energy to escape from the attraction of both asteroids. The L2 escape velocity (v_{L2}) represents the velocity corresponding to the level of energy for which the L2 neck opens. The same considerations made for L1 apply: in this case, in order to escape from L2 neck the minimum escape velocity v_{L2} is about 5.11 cm/s. Figure 4 shows the stable/unstable manifold branches associated to L1 and L2, corresponding respectively, to minimum escape/touch down velocity solutions.

To summarize, no escape is possible for velocities below the L1 point limit v_{L1}, while escape is possible through the L1 neck for $v_{\mathrm{L1}} < v < v_{\mathrm{L2}}$ and through the L2 neck for $v > v_{\mathrm{L2}}$. L1 and L2 escape velocities are reported in Table 2 for different cases of Didymos modeling: escape conditions are compared for the case of sphere-sphere (S1-S2), sphere-ellipsoid (S1-E2) and polyhedron-ellipsoid (P1-E2) models. Note that values differs significantly when Didymoon is modeled as sphere or ellipsoid, while there is no

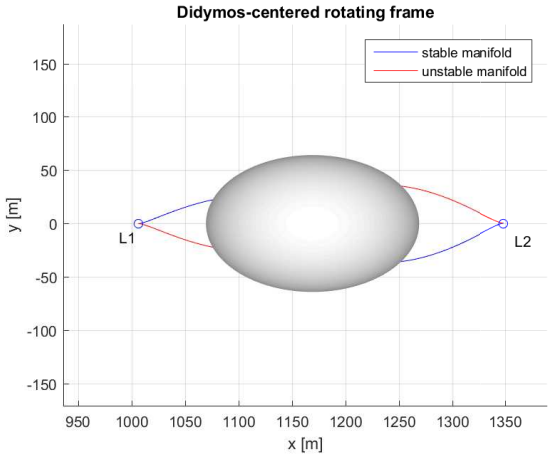

Figure 4: Stable (blue) and unstable (red) manifolds associated to L1 and L2 points. Stable manifolds corresponds to minimum escape velocity solutions, unstable manifolds to minimum touch down velocity solutions

substantial dependency on Didymain's modeling strategy.

Table 2: L1 and L2 escape velocities for different Didymos models: sphere-sphere (S1-S2), sphere-ellipsoid (S1-E2) and polyhedron-ellipsoid (P1-E2) [cm/s].

	S1-S2	**S1-E2**	**P1-E2**
v_{L1}	4.95	4.58	4.57
v_{L2}	5.23	5.11	5.11

Figure 5 shows a Monte Carlo simulation performed to support energy considerations when looking at touch down velocities. A uniform distribution of points is considered on the surface of Didymoon and the dynamics are propagated backwards from each of these points, with a given touch down velocity v at the surface, uniformly distributed in direction. It is shown that no trajectories comes from outside the binary system for touch down velocities below the L1 point limit v_{L1} (Figure 5(a)), while some trajectories exist through the L1 neck for $v_{L1} < v < v_{L2}$ (Figure 5(b)). Trajectories through both L1 and L2 are finally shown for $v > v_{L2}$ (Figure 5(c)).

3.2. The manifold landing strategy

The L1 case is the lower limiting case in terms of energy level of the third body. This solution might be applied to the MASCOT-2 scenario. However,

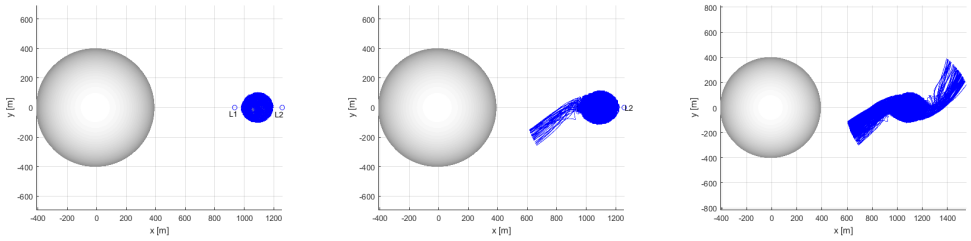

(a) (b) (c)

Figure 5: Monte Carlo simulation: backwards integration of dynamics with initial velocity v from the surface of Didymoon (a) $v < v_{\mathrm{L1}}$, (b) $v_{\mathrm{L1}} < v < v_{\mathrm{L2}}$, (c) $v > v_{\mathrm{L2}}$.

due to safety issues, the L1 solution is discarded in favor of a safer release from L2 side. It is indeed preferable to release the lander from outside the asteroid system (L2 side) rather than from between the two asteroids (L1 side). For these reasons, for MASCOT-2 scenario, low energy trajectories associated to unstable manifold of L2 are investigated as suitable landing solutions. A purely ballistic landing can be achieved by releasing MASCOT-2 from the L2 point, on its unstable manifold. This constraints the release altitude and the AIM spacecraft trajectory to the L2 point. Different and higher release altitudes are desirable from the mission design point of view. To achieve this goal, the design strategy foresees to construct the ballistic descent starting from outside the L2 region, by combining the stable L2 manifold (from release point up to L2) with the unstable manifold (from L2 to Didymoon's surface). The targeted complete ballistic path of MASCOT-2 from release up to touch down is shown in Figure 6(a). The chosen manifold solution is also suitable to address the challenge of reaching Didymoon after release, since it provides minimization of the instability and divergence of the dynamical flow. From a mathematical point of view, the L2 point includes a 2D stable and a 2D unstable manifold branch. This means that, once at L2, when switching from stable to unstable manifold, the lander will have the same probability to fall either on the wrong unstable manifold branch (outgoing from Didymos system) or on the right unstable manifold branch (ingoing towards the surface of Didymoon). Since no trajectory control can be operated by MASCOT-2, the lander is released close to the stable manifold, but not exactly on it. The release point is found after propagating backward the state of the landing point associated to the nominal manifold solution, but considering a higher touch down velocity (same direction). The dynamics are backwards

propagation until the release distance is reached. This procedure increases the robustness of the landing solution, at the cost of a slightly higher energy and touch down velocity.

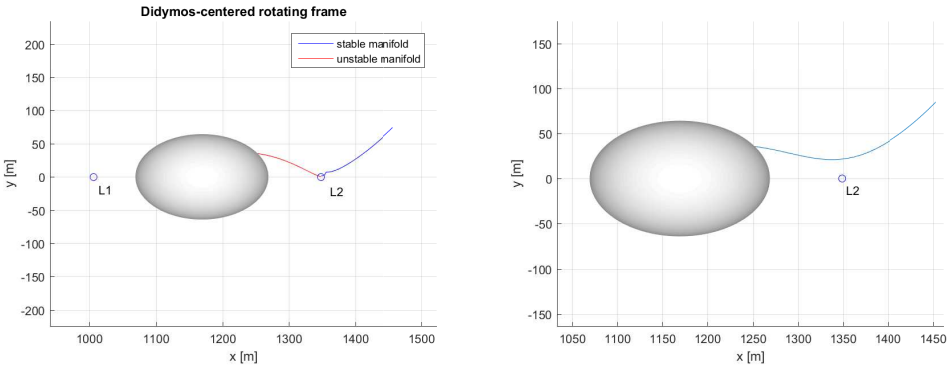

(a) (b)

Figure 6: (a) Stable (blue) manifold branch carries the lander from release point up to L2, where it jumps on the unstable (red) branch to proceed towards the Didymoon's surface. (b) Robust landing trajectory with release in the proximity of L2 stable manifold

The values in Table 2 are important since they represent dynamical constraints for the MASCOT-2 landing problem. Any ballistic trajectory coming from outside the Didymos system towards Didymoon, will reach the asteroid with a touch down velocity that is (equal or) higher than v_{L2}. Since the AIM spacecraft, for safety reason, will not deploy MASCOT-2 too close to the two asteroids, v_{L2} represents the minimum touch down velocity for candidate ballistic trajectories related to the AIM/MASCOT-2 scenario. It is highlighted here that manifolds are computed using the modified CR3BP formulation described in Section 2.

4. Design solution and results

This Section discusses the landing design problem and presents solutions according to the design strategy described in Section 3. Assumptions are first presented according to the AIM case study. The effect of design parameters and their uncertainties is detailed and the nominal landing trajectory is presented. Results in terms of landing success rate and dispersion are eventually shown.

4.1. Assumptions

MASCOT-2 will be released by the AIM spacecraft at a safe distance of 200 m from Didymoon's surface. As discussed in the previous section, the baseline design strategy foresees the exploitation of the manifold dynamics associated to the L2 point. Numbers and figures refer to physical parameters of Didymos system as reported in Pravec et al. (2006). The following paragraphs reports the main assumptions related to the AIM design scenario.

4.1.1. Release

MASCOT-2 will be released by AIM by means of a spring-based mechanism, which will provide a relative velocity between the lander and the orbiter of few cm/s. From the mission design point of view, the chosen ballistic trajectory must be robust to uncertainties in the release event. The nominal trajectory is validated against state dispersion at release. More in detail, errors related to AIM navigation and release mechanism are taken into account and the information is used to assess the success rate of the release. To avoid and mitigate the risk of collision with the asteroids, relative optical navigation is performed by the AIM spacecraft during close-proximity operations. Navigation errors at release are due to the uncertainties in the reconstruction of center of Didymoon and Didymain based on camera images and by Didymoon's surface landmarks matching. The following contributions are considered:

- Navigation error: applied on the full release state (both position and velocity) of AIM spacecraft at release. Dispersions are computed according to AIM navigation information. The amount of navigation error at release is quantified into a position error of 11 m (1σ value) and a velocity error of 0.5 cm/s (1σ value).

- Release mechanism error (vector direction): error in relative velocity between MASCOT-2 and AIM spacecraft at release. The error is dispersed around the nominal release velocity provided by the spring. The error in direction is quantified within a half-cone angle of 5 deg (1σ value) around nominal release direction.

- Release mechanism error (vector norm): the error is quantified into the 10% (1σ value) of the nominal release velocity norm.

4.1.2. Interaction with asteroid surface

An important part of MASCOT-2 landing design is to assess and simulate the dynamics of the lander once it gets in contact with the asteroid's soil. The interaction with Didymoon's surface is a crucial point to establish whether MASCOT-2 will escape or not after bouncing. As mentioned, a successful landing will likely see MASCOT-2 bouncing few times on the surface of Didymoon before coming to a rest. The modeling of the surface interaction heads to the definition of the velocity of MASCOT-2 after touch down.

- Velocity after touch down (norm): the most important aspect to be studied is to assess the quantity of energy dissipated at touch down. This effect can be summarized into a single parameter, called restitution coefficient, defined as the ratio between velocity after (v_{TD}^{+}) and before (v_{TD}^{-}) touch down

$$\eta = \frac{v_{\mathrm{TD}}^{+}}{v_{\mathrm{TD}}^{-}} \tag{3}$$

  The restitution coefficient ranges from 0 (fully inelastic collision) to 1 (fully elastic collision) and it represents a measure of the energy dissipated at contact ($\eta \leq 1$). As for the case of study, two different effects are considered as dissipative terms: part of the energy at touch down will be absorbed by the structure of MASCOT-2 (η_{struct}), part of it will be absorbed by the asteroid's soil (η_{soil}):

$$\eta = \eta_{\mathrm{soil}} \cdot \eta_{\mathrm{struct}} \tag{4}$$

  The restitution coefficient allows to evaluate the amount of energy dissipated by the impact, which essentially turns into a decrease in the norm of the velocity vector after bouncing. The actual parameter, related to the Didymoon/MASCOT-2 scenario, is of course very difficult to be known and it is usually estimated according to the expected surface properties. Missions such as JAXA's Hayabusa Tsuchiyama et al. (2011), ESA's Rosetta Biele and Ulamec (2008); Ulamec et al. (2014) and NASA's NEAR-Shoemaker Veverka et al. (2001) have shown how hard is to accurately estimate such parameter based on the soil's response and that a high level of uncertainty exists. For this reason, a worst case scenario is considered here, with very poor dissipation introduced by a very hard soil ($\eta_{\mathrm{soil}} = 0.9$). The damping effect provided by MASCOT-2 structure was estimated and the overall coefficient of restitution is $\eta = 0.6$.

- Velocity after touch down (direction): uncertainties on the local soil inclination are included in the model to stochastically reproduce the irregularities of the surface. The direction of velocity after touch down is computed according to uniform distribution in azimuth and with gaussian distribution in elevation with mean value of 90 deg and 3σ value dispersion of 70 deg.

4.2. Sensitivity to design parameters

In order to properly design an effective landing trajectory and to be robust to real-world conditions, it is important to identify design parameters critical for the success of the maneuver. This section presents sensitivity analyses performed on the design parameters. Being related to an ongoing mission design, the analyses presented might refer to different phases of design process. Hence, numbers and figures might not be fully consistent with other provided in the text, due to updates on requirements and data available during the design phase. However, the general results in terms of behavior and identification of criticalities hold.

4.2.1. Sensitivity to Didymos properties

A great source of uncertainty could reside in the actual mass of Didymos. In particular, concerning the three-body dynamics, the ratio between the two masses is the relevant parameter. According to available data, current uncertainties on the mass ratio are quantified around the nominal value as follows

$$M_2/M_1 = 0.0093 \pm 0.0013 \tag{5}$$

L1 and L2 escape velocities have been computed for the limiting cases and a variability of about ± 0.6 cm/s around the nominal escape velocities is found. Results show that the higher M_2/M_1, the higher the success rate. A very low value of M_2/M_1 can critically affect the success of the landing maneuver, while no problem is expected for mass ratio equal or greater than its nominal value.

4.2.2. Sensitivity to release conditions

As far as the spacecraft design is concerned, the major source of error in MASCOT-2 trajectory is surely due to uncertainty in release conditions. General sensitivity analyses showed that position error can be tolerated up to tens of meters, while the dynamics imposes a much more stringent requirement on velocity dispersion which cannot be tolerated to be above a few

cm/s. The effects associated to each separate contribution due to navigation, release mechanism error in direction and in norm of velocity vector are investigated. Nominal error are defined, with reference to assumptions reported in the previous section. The relevance of each effect is identified by means of Monte Carlo simulation performed using different values of uncertainty. In the attempt to increase landing performance, lower errors with respect to nominal one are investigated. The aim is to identify critical parameters whose reduction of uncertainty can be effective to increase the landing performance. Monte Carlo simulations are performed using a fraction of the nominal error (10%, 20%,...) associated to the three aforementioned effects when considered separately: when one effect's uncertainty is decreased, the remaining two are taken with their nominal uncertainty. Sensitivity on successful landing probability is shown in Figure 7, for the case of release from 200 m and 300 m altitude. Each point in the curves represents a Monte Carlo simulation performed. Each curve represents the simulations performed while varying one parameter associated to dispersion. The blue line refers to navigation error: several Monte Carlo simulations are ran using nominal (100%) release mechanism errors and variable navigation error, from 10% up to nominal (100%). The percentage is directly applied on the error to be summed to the release state of AIM (both position and velocity). The same applies for the other two cases. The red line refers to variation in the error associated to the norm of release mechanism velocity, which ranges between the 10% of its nominal value (that correspond to 1% of velocity) and its nominal value (10% of velocity) while keeping the other effect as nominal. Finally, the yellow line refers to errors in the direction of release mechanism velocity, which ranges between 10% of its nominal value (half cone angle of 0.5 deg) and its nominal value (half cone angle of 5 deg). Figure 7 shows clearly that the most relevant error that affect the success rate of the landing is due to the norm of release mechanism velocity. It is shown indeed that a decrease in this error gives a substantial increase in success rate. The same is not true for the other errors: the increase of navigation accuracy and the increase in release mechanism direction release accuracy do not affect in a relevant fashion the success of MASCOT-2 landing.

Similarly to what is done with success rate, the sensitivity of landing point location to dispersion is also studied for the cases of release from 200 m and 300 m altitudes. Figure 8 and 9 show the 3σ dispersion of latitude and longitude bands of the landing point for the case of, respectively, release from 200 m and 300 m. The results show that both errors in norm and

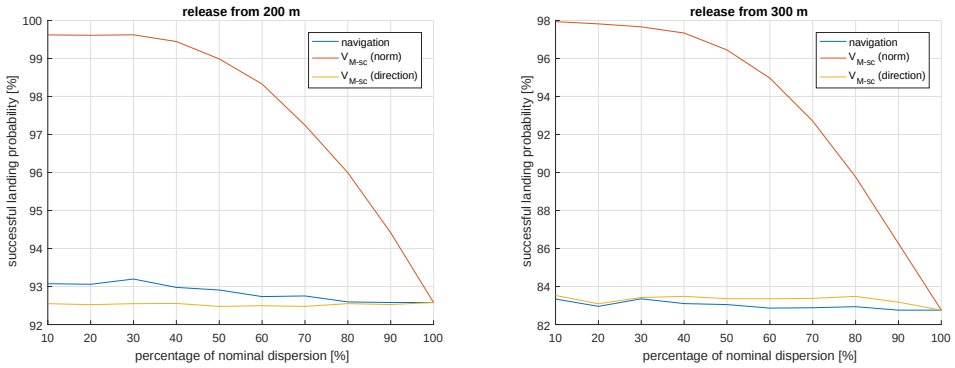

(a) (b)

Figure 7: Successful landing probability with release from (a) 200 m and (b) 300 m altitude

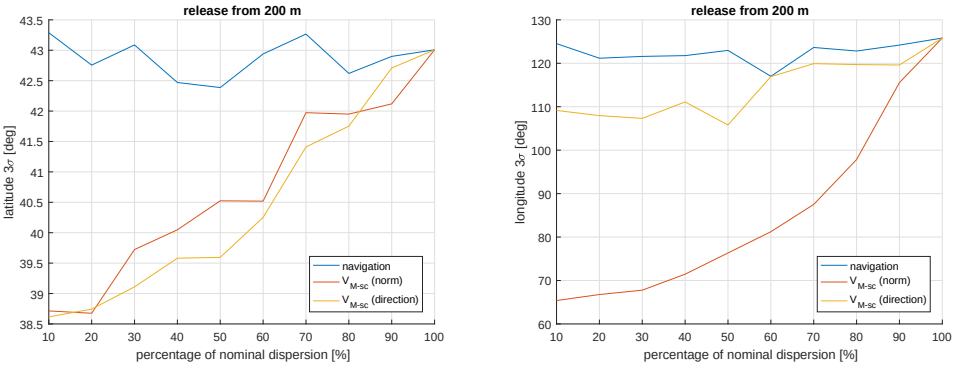

(a) (b)

Figure 8: 3σ dispersion of (a) latitude and (b) longitude bands of landing point with release from 200 m

direction of release mechanism velocity are relevant with respect to dispersion in longitude, while navigation error plays a minor role. Concerning the effects on latitude dispersion, the difference is shown to be very low (about 5 deg) between worst and best cases. The latitude is therefore not very affected by release errors.

As a further relevant parameter to be studied, the sensitivity analysis is also performed on the time of flight during ballistic descent, from release until rest on Didymoon's surface. Figure 10 shows results for the cases under study. As for the case of landing point, the time of flight is shown to be affected by

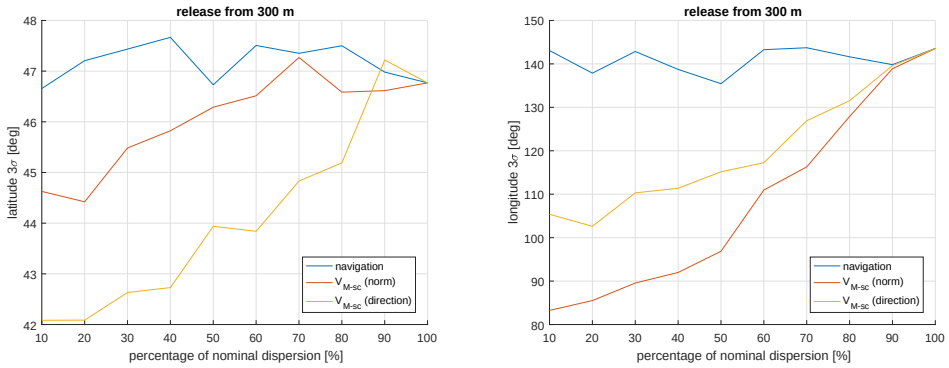

(a) (b)

Figure 9: 3σ dispersion of (a) latitude and (b) longitude bands of landing point with release from 300 m

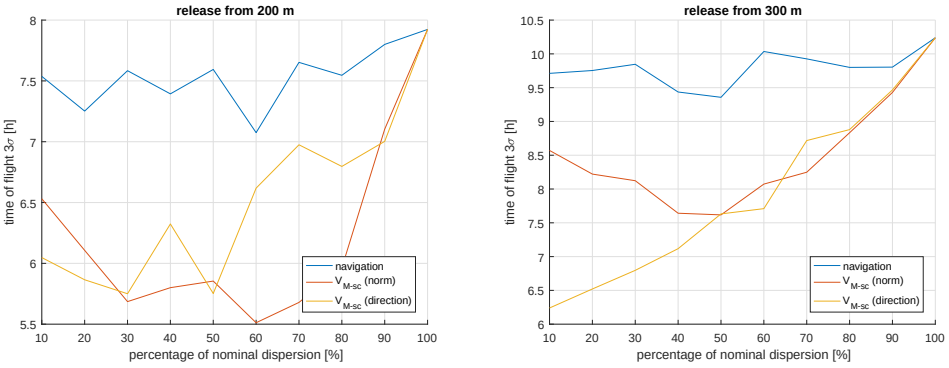

(a) (b)

Figure 10: 3σ dispersion of time of flight until rest on surface with release from (a) 200 m and (b) 300 m altitude

both errors in norm and direction of the release mechanism velocity.

4.2.3. Sensitivity to touch down conditions

A very important issue to be addressed is the assessment of escape probability after touch down. With this respect, the key parameter is the restitution coefficient η, namely the ratio between the velocity of the lander after and before touch down. Results are here presented related to different restitution coefficient to reproduce the interaction between MASCOT-2 and

Didymoon's surface.

- Dissipation of velocity normal to the surface ($\eta_n = 0.5, \eta_t = 1$). In this case the effects of the restitution coefficient are subdivided into tangential and normal contributions. The absolute value of the velocity after touch down is dissipated of $\eta_n = 0.5$ in the direction normal to the surface, while its component tangent to the surface is not dissipated at all ($\eta_t = 1$). To assess the probability of escaping due to bouncing after the first touch down, a Monte Carlo simulation is run. All dispersed landing points (first touch down) are considered. The trajectory after the first bouncing is then computed for each landing point solution by assuming a uniformly distributed direction of velocity vector after touch down. This strategy is driven by the uncertainties in the relative geometry between the lander and the soil at the landing points and it allows to take into considerations all possible inclinations of Didymoon's surface. Figure 11 shows an example of bouncing dynamics until rest. The relevant aspect to be highlighted is that with no dissipation of tangential component of velocity, the lander keeps bouncing towards the equatorial latitude band, with very large longitude footprint.

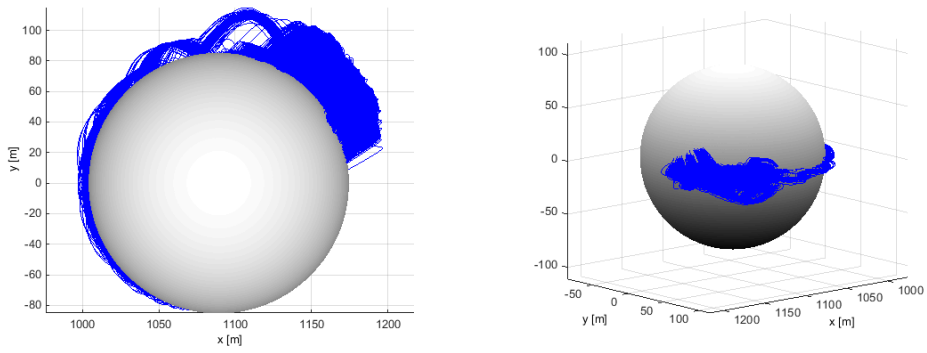

(a) (b)

Figure 11: Bouncing until rest associated to velocity dissipation normal to the surface: (a) x, y view (b) 3D view (early spherical Didymoon model)

- Hard soil and low energy dissipation by MASCOT-2 structure ($\eta = 0.9$). In this case touch down dynamics is modeled using an extremely

conservative assumption for the restitution coefficient. Figure 12(a) shows dispersed trajectories after first touch down for a single bouncing and for a single landing trajectory. The height after bouncing is very high, since very little energy is dissipated after touch down. The dynamics clearly show a westwards trend, since the majority of second landing points are located further west with respect to the first landing point.

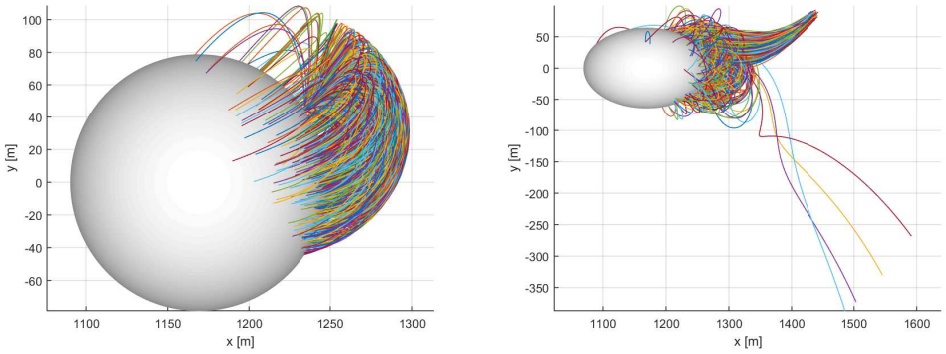

(a) (b)

Figure 12: Hard soil and low structural dissipation case: (a) trajectories after first touch down (early spherical Didymoon model) and (b) bouncing until rest

Figure 12(b) shows an example of full simulation from release up to rest on Didymoon or escape. This specific case refer to very good condition in terms of release, which is very robust since all trajectories reach Didymoon. However, due to the high η and the low dissipation of energy, some of them escape after the first touch down.

4.3. Nominal landing

As discussed, the nominal release strategy is based on the exploitation of manifold dynamics associated to L2. MASCOT-2 will be released near the stable manifold and will transit near L2 to the unstable manifold branch to reach Didymoon's surface. The strategy to compute such trajectory is described and discussed here.

The nominal trajectory is computed starting from the inner branch (between Didymoon and L2) of the unstable manifold solution associated to the

L2 point. The manifold is computed starting from the L2 point and propagating the dynamics forward until the surface of Didymoon is intersected. Unstable L2 manifold dynamics would naturally push the lander towards the surface, even after bouncing. For this reason, the intersection of the manifold with the surface is a favorable location to be targeted for MASCOT-2 landing. As mentioned, a direct release on the stable manifold with transition to the unstable manifold at L2 is not robust from the mission design point of view, since the lander, once at L2, would have a 50% chance to follow either the ingoing or the outgoing manifold branch. For this reason, a higher energy solution is adopted. Due to its favorable location, the landing position identified by the manifold's intersection with Didymoon's surface is kept fixed. The higher energy solution is found by increasing the velocity at touch down and by integrating the dynamics backwards, until the desired release distance from Didymoon is reached. Higher energy trajectories generated through this strategy are shown in Figure 13 to cross the upper part of the L2 neck of the Hill's curves. This region is close to the stable ingoing branch of the L2 manifold. The trajectories found are natural connections between the stable ingoing L2 manifold and the unstable ingoing L2 manifold and fits with the goal of the design strategy.

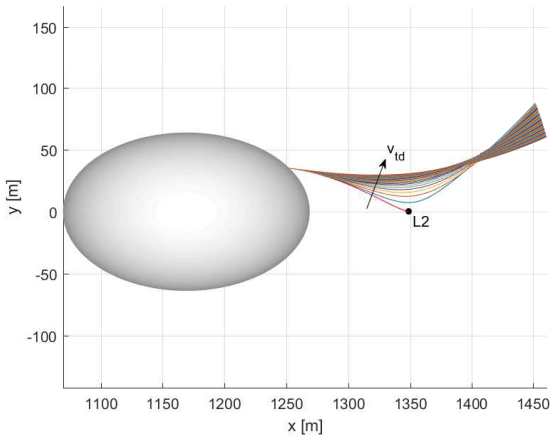

Figure 13: Landing trajectories based on unstable L2 manifold solution for increasing touch down velocities.

The drawback of choosing a higher energy solution is that, due to a higher touch down velocity, the risk the lander escapes after bouncing is higher. However, analyses and investigations performed have shown that favorable

conditions near the unstable manifold landing point guarantee very low risk of escape. After extensive investigation on sensitivity due to the different parameters involved in the design, a touch down velocity of about 6.2 cm/s was selected to generate the nominal ballistic landing trajectory.

4.3.1. Optimal AIM release conditions

As discussed, landing release uncertainties depend both on release mechanism and on AIM spacecraft navigation. Uncertainty in release position is only dependent on AIM navigation accuracy, whereas uncertainty in release velocity is due to the combined effect between AIM navigation accuracy and release mechanism accuracy. Figure 14 shows examples of release velocities, referring to two different release strategies (plain and dashed arrows). $\boldsymbol{V}_{\mathrm{M}}$ indicates the velocity of MASCOT-2 at release in the synodic three-body reference frame. This value is common for both strategies, since it is chosen a priori in order to release the lander near manifold dynamics and it is provided by the initial condition on the nominal landing trajectory. $\boldsymbol{V}_{\mathrm{M}}$ is then a constraint from the design point of view, to ensure high landing successful probability. $\boldsymbol{V}_{\mathrm{sc}}$ is the velocity of AIM spacecraft, while $\boldsymbol{V}_{\mathrm{M\text{-}sc}}$ is the relative velocity between MASCOT-2 and AIM spacecraft. The following vectorial relation holds:

$$\boldsymbol{V}_{\mathrm{M}} = \boldsymbol{V}_{\mathrm{sc}} + \boldsymbol{V}_{\mathrm{M\text{-}sc}} \tag{6}$$

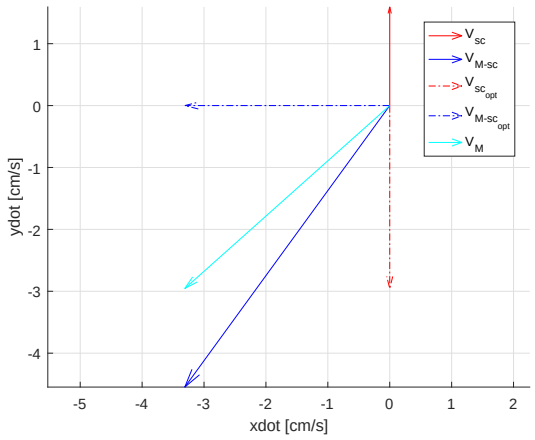

Figure 14: Release velocities: optimal release (dashed) compared to general one (plain).

As mentioned, the error in the norm of the release velocity $\boldsymbol{V}_{\mathrm{M\text{-}sc}}$ due to

spring mechanism equals the 10% (1σ) of its nominal value. For this reason, it is convenient to minimize $\|\boldsymbol{V}_{\text{M-sc}}\|$ when designing AIM release conditions. The term *optimal* refers here to release conditions that minimize the errors at the release event. The minimization includes the fulfillment of some constraints: $\boldsymbol{V}_{\text{M}}$ is constrained since it represents the initial conditions for the ballistic descent close to the stable L2 manifold. Also, for safety reasons, AIM is constrained on a hyperbolic-kind orbit (patched-conics assumptions), with pericenter at release point. In that case, $\boldsymbol{V}_{\text{sc}}$ is constrained to be orthogonal to the x axis and aligned to the y axis. Given such constraints together with Eq. (6), the optimal release condition occur when $\boldsymbol{V}_{\text{M-sc}}$ is aligned with the x axis and equal to the x component of $\boldsymbol{V}_{\text{M}}$, while $\boldsymbol{V}_{\text{sc}}$ equals the y component of $\boldsymbol{V}_{\text{M}}$. It can be easily proven that this condition minimizes $\|\boldsymbol{V}_{\text{M-sc}}\|$ and consequently minimizes the 10% error on it.

4.4. Landing success rate

The results presented here refer to the nominal trajectory case, under the assumptions related to the mission scenario under study. The robustness of the ballistic landing solution is validated against release and touch down uncertainties, to guarantee the success of the landing strategy. A Monte Carlo analysis is performed to assess successful landing probability. The dispersed release conditions are propagated forward using the hi-fidelity polyhedron/ellipsoid three-body model described in Section 2. The dynamics of the lander are propagated until MASCOT-2 comes to a rest on Didymoon's surface, or escapes from Didymos system. Bouncing dynamics is modeled as described above and the resting condition is associated to the residual vertical velocity of the lander after bouncing. More into detail, MASCOT-2 is considered at rest when its vertical velocity is lower than 0.5 cm/s.

Monte Carlo analysis is run with 200 000 points for each different release altitude under study. More in detail, release altitudes of 100, 150, 200, 250 and 300 m from Didymoon's surface are considered.

Figure 15 shows an example of dispersed release conditions and landing trajectories associated to the case of 200 m altitude release. The figure is included only for visualization purpose, since only 200 trajectories (out of 200 000) are displayed.

Table 3 shows the percentage of escaped trajectory after release dispersion, for all considered release altitudes. Escape rate is divided into escaped after release and escaped after touch down. In the first case, the uncertainty drives MASCOT-2 on a different path, which, due to the extremely chaotic nature

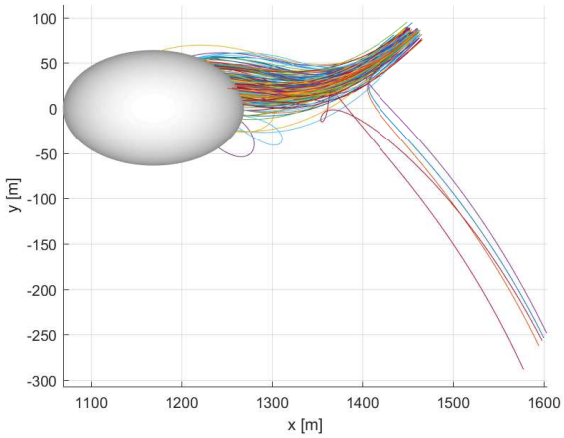

Figure 15: Dispersed landing trajectories from release altitude of 200 m.

Table 3: Escape probability from Didymoon.

Release altitude [m]	Escaped trajectories [%] after release	after touch down	TOTAL
100	1.14	0.00	1.14
150	1.26	0.00	1.26
200	3.18	0.01	3.19
250	5.79	0.04	5.83
300	6.03	0.32	6.35

of the dynamics, does not allow the lander to reach the surface of Didymoon. The second case accounts for MASCOT-2 state after first touch down and in particular, for the cases when the lander is put on an escape trajectory after bouncing on the asteroid. As expected, the success rate of the ballistic landing increases as the release altitude decreases. Successful probability ranges from a worst case value of 93.65% for release from 300 m altitude, to a maximum of 98.86% in the case of release from 100 m altitude. Results in terms of success rate are in agreement with a similar analysis performed by DLR Tardivel et al. (2016) on MASCOT-2 landing probability.

4.5. Landing dispersion

After assessing the successful rate of the release strategy, it is important to study the outcome of the successful landing in terms of final landing point dispersion. Table 4 reports the latitude and longitude bands related to MASCOT-2's point at rest on Didymoon, for the different release altitude

cases. The Time of Flight (ToF) during ballistic descent and bouncing, from release up to rest on Didymoon is also reported. Uncertainty range is included and specified according to a Gaussian 3σ distribution.

Table 4: Landing dispersion on Didymoon's surface at rest: latitude/longitude bands and time of flight between release and rest.

Release altitude [m]	Dispersion at rest [$\mu \pm 3\sigma$] Latitude [deg]	Longitude [deg]	ToF [h]
100	0.2 ± 32.5	23.3 ± 87.9	1.81 ± 0.95
150	0.0 ± 31.5	20.1 ± 66.7	2.19 ± 1.06
200	0.1 ± 32.9	19.7 ± 60.5	2.50 ± 1.21
250	-0.1 ± 36.6	20.5 ± 64.8	2.77 ± 1.41
300	0.1 ± 44.3	19.5 ± 86.0	2.95 ± 1.35

With reference to the case of 200 m release altitude in Table 4, Figure 16 shows the landing dispersion on the surface of Didymoon when the lander is at rest. More in detail, the latitude-longitude map is shown in Figure 16(a), while the three-dimensional view of all landing points on Didymoon's surface is shown in Figure 16(b). Latitude and longitude distributions of resting point are displayed, respectively, in Figure 16(c) and 16(d).

It must be highlighted that the dynamical behavior of the lander after touch down is heavily dependent on the choice of the restitution coefficient η. According to latest assumptions on release parameters and restitution coefficient, the results show that the landing region can be estimated within an uncertainty in the latitude-longitude region on the order of tens of degrees. This allows to state that the lander will likely come to a rest in the hemisphere of Didymoon opposite to Didymain.

5. Conclusion

As mentioned in the previous sections and proved by the results and analyses presented, the problem of MASCOT-2 landing is extremely challenging. A summary of the problem's criticalities is provided here. Two main critical aspects can be identified: the first is related to the capability of MASCOT-2 to reach Didymoon after release and a pure ballistic landing. The second is related to the capability of MASCOT-2 of staying on the surface of Didymoon after touch down, without escaping from its weak gravity attraction. Relevant design parameters and physical properties of Didymos affecting such capabilities are summarized here.

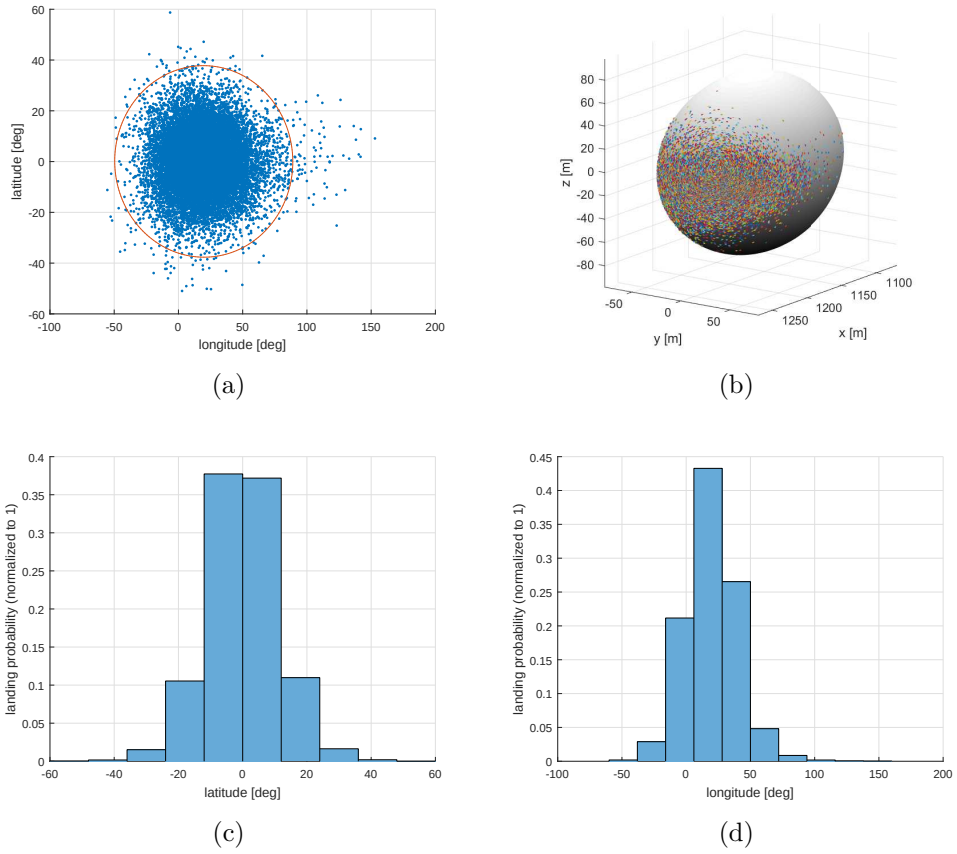

Figure 16: Landing dispersion at rest for the case of 200 m altitude release. (a) latitude-longitude map (b) three-dimensional view of Didymoon (c) latitude and (d) longitude distribution of points.

5.1. Capability to reach Didymoon

Reaching Didymoon is the most critical aspect regarding MASCOT-2 descent because the gravity environment around the Didymos binary system is extremely chaotic, and a very small deviation of release conditions can drive the lander far from Didymoon. The most relevant parameters are:

- Mass distribution among Didymos system (mass ratio between Didymoon and Didymain): it is shown that the higher M_2/M_1, the better it is in terms of success rate. This parameter can be very critical for values $M_2/M_1 < 0.0093$ (nominal up-to-date value), while not critical for $M_2/M_1 \geq 0.0093$

- Nominal release: it is extremely important to select the release point conditions in Didymoon three-body system. As discussed, nominal release is chosen exploiting manifold dynamics associated to the L2 point. The success rate decreases dramatically and the landing can never be achieved when manifold dynamics is not exploited.

- Release uncertainties: as discussed, position uncertainty is not an issue and can be tolerated up to tens of meters. On the other hand, velocity dispersion can be very critical for values above few cm/s. More into detail, sensitivity analyses performed showed that uncertainties due to the norm of velocity release mechanism can be very critical concerning the success rate of the landing maneuver. A strategy to mitigate such effect is discussed here.

5.1.1. Capability to stay on Didymoon

Staying of Didymoon after touch down is very critical for MASCOT-2 landing design, due to the very low gravity attraction of Didymoon and, consequently, to its very low escape velocity. Relevant parameters to this problem are:

- Mass ratio between Didymoon and Didymain: the escape velocity increases as the mass of Didymoon increases. Analogously to the previous case, the higher M_2/M_1, the better it is.

- Restitution coefficient: this parameter is the key parameter to model the interaction between the soil and MASCOT-2. It is shown to be very critical for values $\eta > 0.7$, while not critical for $\eta \leq 0.7$.

- Uncertainty in soil inclination: this has shown not to be critical in terms of success rate.

- Nominal release: due to its peculiar dynamics, the escape velocity from the surface of Didymoon is not constant but it depends on latitude and longitude. For this reason it is very important to land on a region with low escape velocity. As discussed in Section 3, such region is that associated to unstable manifold dynamics. As for the case selected, unstable manifold dynamics associated to the L2 point provide a low energy solution (low touch down velocity) that pushes MASCOT-2 away from L2 point, and then towards Didymoon's surface, even after touch down.

Acknowledgement

The work presented here has been performed under ESA contract during the phase A/B1 of AIM study.

References

Bellerose, J. and Scheeres, D. J. (2008a). General dynamics in the restricted full three body problem. *Acta Astronautica*, 62:563–576.

Bellerose, J. and Scheeres, D. J. (2008b). Restricted full three-body problem: Application to binary system 1999 kw4. *Journal of Guidance, Control, and Dynamics*, 31(1):162–171.

Belton, M. J. S., Chapman, C. R., Veverka, J., et al. (1994). First images of asteroid 243 ida. *Science*, 265(5178):1543–1547.

Biele, J. and Ulamec, S. (2008). Capabilities of philae, the rosetta lander. *Space Science Reviews*, 138(1):275–289.

Bottke Jr., W. F., Cellino, A., Paolicchi, P., and Binzel, R. P. (2002). *Asteroids III*. Space Science Series. University of Arizona Press, Tucson, AZ.

Cheng, A., Atchison, J., Kantsiper, B., et al. (2015). Asteroid impact and deflection assessment mission. *Acta Astronautica*, 115:262–269.

Colagrossi, A., Ferrari, F., Lavagna, M., and Howell, K. (2016). Dynamical evolution about asteroids with high fidelity gravity field and perturbations modeling. In Turner, J., Wawrzyniak, G., Cerven, W., and Majji, M., editors, *Advances in the Astronautical Sciences (Proceedings of the AIAA/AAS Astrodynamics Specialist Conference)*, volume 156, pages 885–903, Napa, CA, USA. Univelt Inc.

Ferrari, F., Lavagna, M., Carnelli, I., et al. (2016a). Esa's asteroid impact mission: Mission analysis and payload operations state of the art. In *Proceedings of the 6th International Conference on Astrodynamics Tools and Techniques*, (online at https://indico.esa.int/indico/event/111), Darmstadt, DE.

Ferrari, F., Lavagna, M., and Howell, K. C. (2016b). Dynamical model of binary asteroid systems through patched three-body problems. *Celestial Mechanics and Dynamical Astronomy*, 125(4):413–433.

Ferrari, F., Tasora, A., Masarati, P., and Lavagna, M. (2017). N-body gravitational and contact dynamics for asteroid aggregation. *Multibody System Dynamics*, 39(1):3–20.

Gabern, F., Koon, W. S., and Marsden, J. E. (2006). Parking a spacecraft near an asteroid pair. *Journal of Guidance, Control, and Dynamics*, 29:544–553.

Geissler, P., Petit, J., Durda, D. D., et al. (1996). Erosion and ejecta reaccretion on 243 ida and its moon. *Icarus*, 120(1):140 – 157.

Hilton, J. L. (2002). Asteroid masses and densities. In Bottke Jr., W. F., Cellino, A., Paolicchi, P., and Binzel, R. P., editors, *Asteroids III*, pages 103–112. University of Arizona Press, Tucson, AZ.

Kaula, W. M. (1966). *Theory of Satellite Geodesy: Applications of Satellites to Geodesy*. Special series of brief books covering selected topics in the Pure and applied sciences. Blaisdell Pub. Co., Waltham MA.

Margot, J. L., Nolan, M. C., Benner, L. A. M., et al. (2002). Binary asteroids in the near-earth object population. *Science*, 296:1445–1448.

Merline, W. J., Weidenschilling, S. J., Durda, D. D., et al. (2002). Asteroids do have satellites. In Bottke Jr., W. F., Cellino, A., Paolicchi, P., and Binzel, R. P., editors, *Asteroids III*, pages 289–312. University of Arizona Press, Tucson, AZ.

Muller, P. M. and Sjogren, W. L. (1968). Mascons: Lunar mass concentrations. *Science*, 161(3842):680–684.

Pravec, P., Scheirich, P., Kušnirák, P., et al. (2006). Photometric survey of binary near-earth asteroids. *Icarus*, 181:63–93.

Schaub, H. and Junkins, J. L. (2003). *Analytical Mechanics of Aerospace Systems*. AIAA education series. American Institute Of Aeronautics & Astronautics, Reston, VA.

Scheeres, D. J. (1994). Dynamics about uniformly rotating triaxial ellipsoids: Applications to asteroids. *Icarus*, 110:225–238.

Scheeres, D. J. and Bellerose, J. (2005). The restricted hill full 4-body problem: Application to spacecraft motion about binary asteroids. *Dynamical Systems: An International Journal*, 20(1):23–44.

Scheeres, D. J., Ostro, S. J., Hudson, R. S., DeJong, E. M., and Suzuki, S. (1998). Dynamics of orbits close to asteroid 4179 toutatis. *Icarus*, 132:53–79.

Scheirich, P. and Pravec, P. (2009). Modeling of lightcurves of binary asteroids. *Icarus*, 200:531–547.

Sierks, H., Barbieri, C., Lamy, P. L., et al. (2015). On the nucleus structure and activity of comet 67p/churyumov-gerasimenko. *Science*, 347(6220):1044/1–1044/5.

Szebehely, V. (1967). *Theory of Orbits: The Restricted Problem of Three Bodies*. Academic Press, New York and London.

Tardivel, S., Lange, C., Ulamec, S., and Biele, J. (2016). The deployment of mascot-2 to didymoon. In *Proceedings of the 26th AAS/AIAA Space Flight Mechanics Meeting*, number AAS 16-219, Napa, CA, USA.

Taylor, M. G. G. T., Alexander, C., Altobelli, N., et al. (2015). Rosetta begins its comet tale. *Science*, 347(6220):387–387.

Tsuchiyama, A., Uesugi, M., Matsushima, T., et al. (2011). Three-dimensional structure of hayabusa samples: Origin and evolution of itokawa regolith. *Science*, 333(6046):1125–1128.

Ulamec, S., Biele, J., Bousquet, P.-W., et al. (2014). Landing on small bodies: From the rosetta lander to mascot and beyond. *Acta Astronautica*, 93:460–466.

Veverka, J., Farquhar, B., Robinson, M., et al. (2001). The landing of the near-shoemaker spacecraft on asteroid 433 eros. *Nature*, 413:390–393.

Werner, R. A. and Scheeres, D. J. (1997). Exterior gravitation of a polyhedron derived and compared with harmonic and mascon gravitation representations of asteroid 4769 castalia. *Celestial Mechanics and Dynamical Astronomy*, 65:313–344.